Direct 3-D Imaging of the Evolution of Block Copolymer Microstructures Using Laser Scanning Confocal Microscopy

4 AUTHORS, INCLUDING:

Wonmok Lee
Sejong University
59 PUBLICATIONS **1,321** CITATIONS

SEE PROFILE

Hyunjung Lee
Kookmin University
34 PUBLICATIONS **855** CITATIONS

SEE PROFILE

Edwin L Thomas
Rice University
620 PUBLICATIONS **24,424** CITATIONS

SEE PROFILE

Direct 3-D Imaging of the Evolution of Block Copolymer Microstructures Using Laser Scanning Confocal Microscopy

Wonmok Lee,[†] **Jongseung Yoon,**[‡] **Hyunjung Lee,**[§] **and Edwin L. Thomas***

Department of Materials Science and Engineering, Massachusetts Institute of Technology, Cambridge, Massachusetts 02139

Block copolymers (BCPs) exhibit various periodic structures created through microphase separation with tunable size and shape of microdomains via choice of molecular weight, composition, and chain architecture and with the addition of plasticizers or homopolymers.[1] In order to tailor the desired properties of BCPs, it is critical to gain a fundamental understanding of the 3D structural details of these materials.[2] Various microscopic tools such as transmission electron microscopy (TEM), scanning electron microscopy (SEM), and atomic force microscopy (AFM) have been utilized to extract detailed morphological information on BCPs. TEM has been extensively used for a real-space characterization of self-assembled BCP morphology due to its superior imaging capability down to near atomic length scales.[3] TEM imaging of BCPs, however, requires preparation of a very thin sample (<100 nm) for electrons to pass through, but organic specimens are often subject to electron beam damage (i.e., mass loss and dimensional changes). Because polymers have similar electron densities, selective staining of a specific domain may be required. Each TEM image is a 2D projection of the finite sample thickness along the incident beam direction so information on the 3D microstructure requires a systematic tilt series. SEM is useful for obtaining a 3-D image of the BCP microstructure if the sample can be suitably etched.[4] However, both TEM and SEM cannot follow morphological changes of a specific area due to the cross-linking from the electron beam. Besides electron microscopy techniques, AFM is a useful tool in the study of near-surface morphologies of BCPs, providing information about surface topography (height-image) and surface properties of the different domains (phase-image)[5−8] as well as serial sequences on the evolution of defects.[6] Recently, BCPs have also been characterized by transmission near field scanning optical microscopy (NSOM), which was the first attempt at optical imaging of BCP morphology.[9] In that study, individual lamellar microdomains and defect structures of poly(styrene-*b*-isoprene) (PS-*b*-PI) BCP were characterized using NSOM with polarization modulation polarimetry.

These real-space characterization methods mentioned above are, however, not very suitable for tracking dynamic processes of phase behavior of block copolymers in bulk in real time. Given these limitations of the various microscopy tools, most previous studies on the evolution of BCP microstructure have been conducted using various scattering methods (especially light and X-ray) which can follow the change of morphology in situ,[10−12] but scattering methods have limitations on determination of the complete 3-D structure and to investigate the local nonperiodic structures that often nucleate transformations and control properties.

Laser scanning confocal microscopy (LSCM) is an optical microscopic technique capable of 3-D imaging of microstructures in a nondestructive manner and has been widely used in biology and medicine.[13] In LSCM, a 2-D optical image is generated by performing a raster scan of focused laser probe across a focal plane. The optical signal emanating from the focal spot is sent to a photon detector through confocal pinhole such that out-of-focus signals are effectively eliminated. In this manner, 2-D optical sections collected at different focal planes can be recorded to provide a 3-D image of a thick ($t <$ 100 μm) specimen. LSCM has been successfully employed for 3-D imaging of various systems such as living cells,[14,15] colloidal crystals,[16,17] and liquid crystalline domain structures.[18] LSCM was also used for morphological studies of polymeric materials such as homopolymer gel[19] and polymer blends.[20] Because of the resolution limit of LSCM, which is imposed by diffraction of the probe light, typical BCPs that have a microdomain period of several tens of nanometers cannot be imaged by LSCM. Recently, ultrahigh molecular weight ($\sim 10^6$ g/mol) BCPs have been successfully prepared for creating photonic crystals.[4,21−23] Since the microdomain size of these "photonic" BCPs is large enough to interact with visible light, they can be also characterized using the LSCM technique.[24] In this communication, we report a 3-D optical imaging of high molecular weight BCP morphologies including following dynamic microstructural changes in real space enabled with reflection-mode LSCM.

The photonic PS-*b*-PI BCPs with lamellar and cylindrical morphologies were prepared by anionic polymerization, in which styrene and isoprene monomers were added sequentially in cyclohexane/benzene mixed solvent.[24] When a polymerization proceeded for a sufficiently long time, the reaction mixture began to exhibit reflective colors as the synthesized block copolymer chains self-assemble at an order-to-disorder transition concentration and diffract light of a range of wavelengths corresponding to their photonic stop band.[21] The molecular weight and composition of the BCPs are 8.4×10^5 g/mol (PDI: 1.08) and 57/43 (PS/PI, w/w) for the lamellar-forming BCP (SI_{LAM}) and 1.15×10^6 g/mol (PDI: 1.05) and 22/78 (PS/PI, w/w) for the cylinder-forming BCP (SI_{CYL}) as determined by gel permeation chromatography (GPC) and nuclear magnetic resonance (NMR) analysis. Figure 1a shows a TEM micrograph (JEOL 200CX operated at 100 kV) of a cryo-microtomed sample of slow-cast and annealed (130 °C in vacuum, 24 h) SI_{LAM} after staining in OsO_4 for 3 h. The lamellar period is $\sim$200 nm (110 nm for PS and 90 nm for PI).

Films (thickness $\sim$50 μm) of the lamellar and cylindrical BCP (SI_{LAM} and SI_{CYL}) were prepared by casting the BCP solutions in toluene between a slide-glass and a cover-glass. Since the PS-*b*-PI BCP does not contain any fluorophore, the samples were investigated by reflection mode LSCM in which reflection signals of the probe light (λ = 488 nm) were scanned through an oil-immersion objective lens (Leica, HCX PL APO 63×/ 1.40−0.60). In reflection mode LSCM, incident light is reflected at the interfaces between domains having different indices of refraction. Reflection mode LSCM can be applied to the imaging

---

* Corresponding author. E-mail: elt@mit.edu.
† Current address: Samsung Advanced Institute of Technology, Yongin-si, Gyeonggi-do, Korea.
‡ Current address: Department of Materials Science and Engineering, University of Illinois at Urbana-Champaign, IL 61801.
§ Current address: Korea Institute of Science and Technology, Hawolgok-dong, Seongbuk-gu, Seoul, Korea.
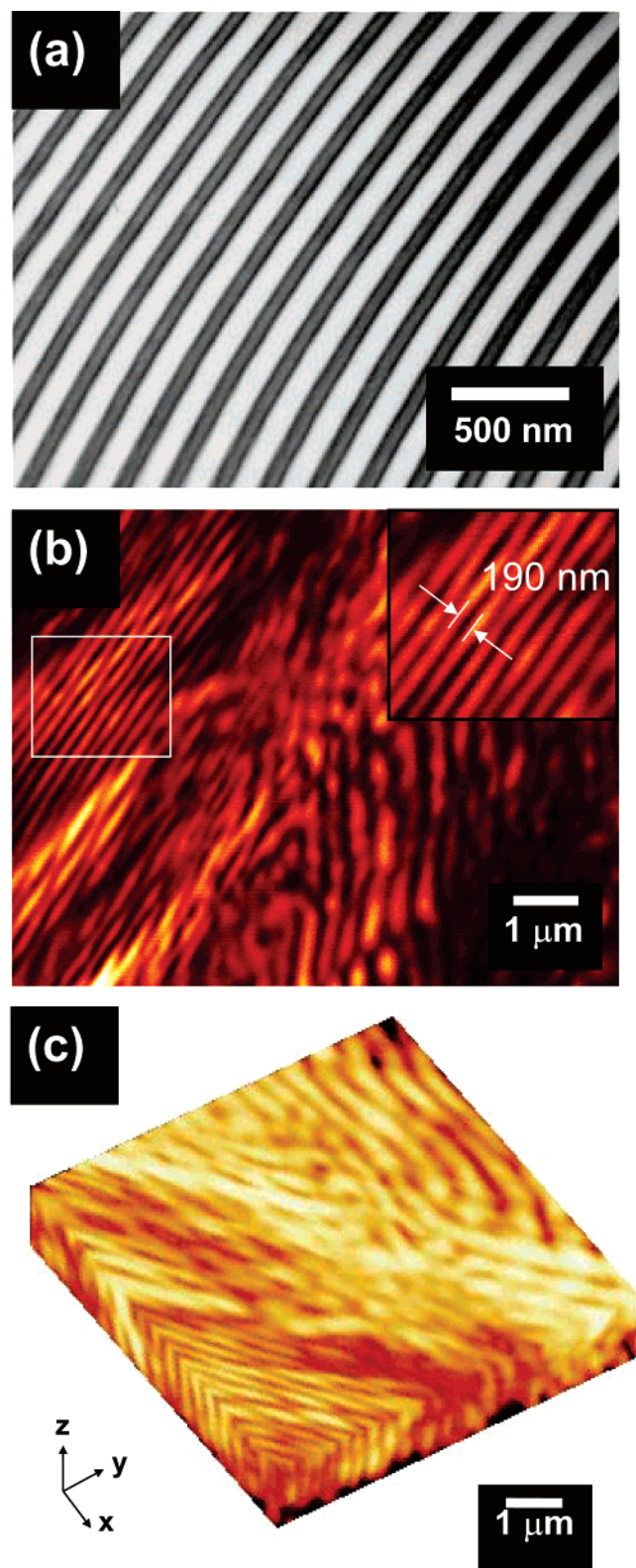
Figure 1. (a) TEM micrograph of SI_{LAM} showing the lamellar morphology, where dark regions correspond to PI domains stained with OsO_4 and the bright regions correspond to PS domains. (b) Reflection mode LSCM images (*xy*-scan) of dried, as-cast SI_{LAM} BCP showing lamellar morphology in a 50 μm film between glass substrates. Ar ion laser probe operated at 488 nm was scanned near the center of the film. (c) 3-D LSCM micrograph of the microdomain structure of SI_{LAM} near the center of the film generated by accumulating 20 reflection mode LSCM images (*xy*-scan) taken at different axial (*z*) position with a depth increment (Δz) of 122 nm.

of various nonfluorescing species such as nonlabeled cells,[25] colloidal particles,[17] and block copolymers.[24] The small refrac-

tive index contrast ($\Delta n = 0.08$) between the PS and PI microdomains enabled the probe light to pass through the sample without a significant scattering loss and to collect the morphological information. Figure 1b shows a reflection mode LSCM micrograph of a dried as-cast SI_{LAM} film. The LSCM image shows a lamellar morphology composed of domains with various lamellar orientations, which was obtained near the center of the sample. Locations that display larger spacing represent regions of tilted lamellae while the magnified region in Figure 1b is of lamellae oriented with their normals parallel to the substrate. The domain periodicity of perpendicularly ordered lamellae is about 190 nm, which is in a fairly good agreement with the value obtained from TEM.

The cylinder-forming BCP (SI_{CYL}) could be also imaged at the domain level by LSCM.[24] A 50 μm thick film of the dried and annealed SI_{CYL} sample was examined by reflection-mode LSCM and showed the variation of the microdomain orientation with respect to the distance from the substrate/superstrate (see the Supporting Information). When LSCM images were taken near the polymer−glass superstrate ($\sim$1 μm depth from the upper surface), the cylindrical microdomains that are oriented parallel to the substrate were mostly observed due to the surface effect while the images taken near the center of the film thickness (20 μm depth from the upper surface) displayed more random grain orientations including perpendicularly ordered cylindrical domains.

Two unique features of the LSCM technique are (1) its capability of 3-D depth profiling and (2) its ability to monitor dynamic morphological phenomena in real space. When a series of 2-D lateral images (*xy*-plane) are scanned at different depths, one can graphically reconstruct a 3-D profile of the sample as shown in Figure 1c. To obtain this 3-D LSCM micrograph, 20 *xy*-images were taken from the SI_{LAM} sample with different *z*-positions ($\Delta z = 122$ nm) near the same sample position where Figure 1b was obtained. (A typical 3D image acquisition time is about 20 s for a stack of 20 slices, each *x*, *y* slice having 512×512 pixels.) Viewed from cross-sectional planes (i.e., *xz*- and *yz*-plane), it is evident the lamellar domain interfaces are tilted with respect to the *z*-axis. LSCM also allows a real-time observation of dynamic phase behavior of BCPs due to the fast scanning rate (less than 1 s per frame) and the nondestructive imaging mechanism. As an example, we investigated a BCP gel composed of SI_{LAM} and cumene confined between two circular glass substrates while solvent evaporation occurs along the radial direction. First, a small aliquot of SI_{LAM} solution in cumene ($\sim$20 wt % of polymer) was placed between a microscope slide and a coverslip having a diameter of 18 mm. The sandwiched BCP gel showed a bluish-green reflective color above its order−disorder concentration (ODC) and was examined under LSCM 5 h later. Parts a and b of Figure 2 are lateral (*xy*-plane) LSCM images of SI_{LAM} taken at the mid-position of the sample thickness, at the sample center ($r \sim 0$ mm) and near the sample edge ($r \sim 7$ mm). As shown in Figure 2c, the sample exhibits rainbowlike colors by reflecting a different range of visible light depending on the radial position of the sample. The corresponding cross-sectional (*xz*-plane) LSCM images are shown in Figure 2d,e, and a schematic representation of the cross section of the sample is depicted in Figure 2f.

It is interesting to note that the thickness of the confined BCP gel varies with radial position. The observed film thickness variation may be explained by a combination of two factors: (1) As solvent evaporation occurs, a concentration gradient along the radial direction develops (the arrow in Figure 2c) and mass transport of polymers molecules occurs from the center toward
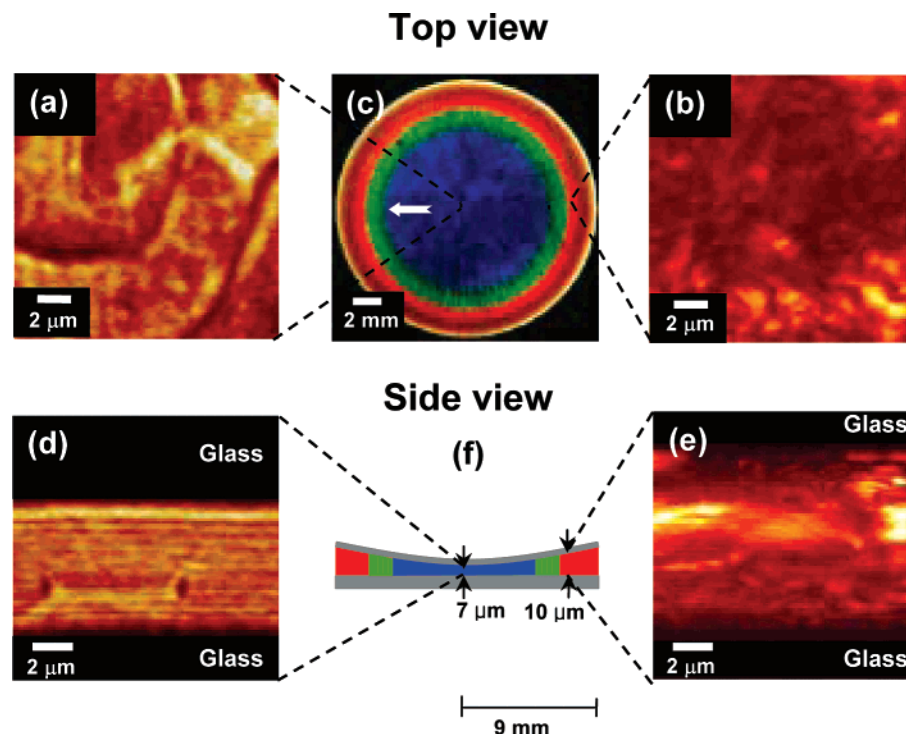
Figure 2. Reflection mode LSCM images of the thin layers of SI_{LAM}/cumene gel sandwiched between two glass slides. The images were captured 5 h after initial sample preparation. (a) and (b) show in-plane LSCM images (xy-scan) taken at the center ($r \sim 0$ mm) and near the edge ($r \sim 7$ mm) of the sample, respectively, and (c) is a photographic image for the top view of the sample with black background under white light illumination. The images (d) and (e) are cross-sectional LSCM images (xz-scan) taken at the center and the near the edge, respectively. The thickness variation of the sample along the radial direction is schematically represented in (f) to help readers understand the sample configuration better, a length scale along thickness (z) direction is exaggerated. Note that due to the increased segment−segment interaction and the radial material flow during solvent evaporation, the total film thickness is 43% thicker near the edge than at the center.
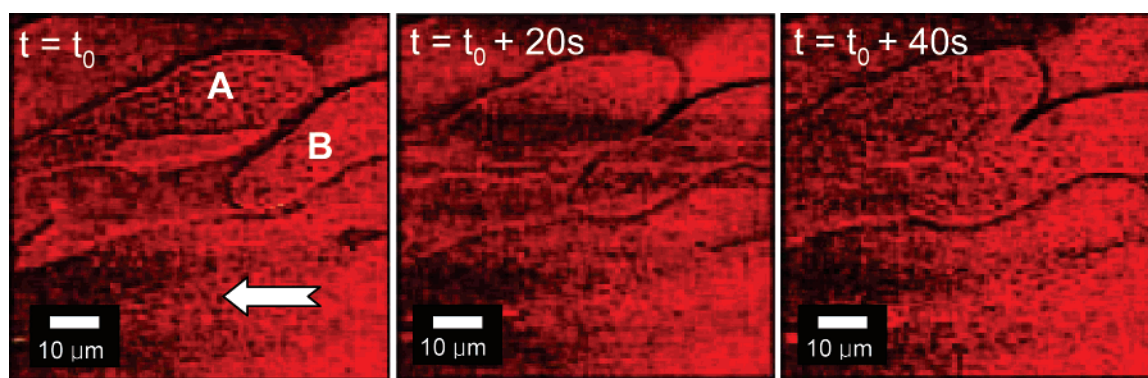
Figure 3. Reflection mode in-plane (xy-scan) LSCM images of SI_{LAM}/cumene mixture taken every 20 s. Three consecutive xy-scans show merging of two lamellar domains while slowly moving together in the direction of concentration gradient. The arrow indicates the direction of motion of the lamellar microdomains.

the edge (vide infra). (2) As the solvent content in the BCP gel decreases, the effective segregation strength (or Flory−Huggins interaction parameter, χ_{PS-PI}) between the unlike blocks increases,[26] and therefore the BCP chains become more extended near the sample edge, resulting, for example, in the increase of macroscopic film thickness from ~ 7 μm at the center to ~ 10 μm at a position 2 mm from the edge. A more detailed treatment for this solvent effect upon microstructure and optical properties of photonic BCPs will be provided in a separate publication. LSCM also reveals that the lamellar microdomains become somewhat disrupted as the film dries: initially excellent parallel microdomain orientation is observed near the center of the sample, while expansion of the layers and mass-transport thickening during solvent evaporation causes layer tilt. Note in Figure 2 that the resolution of LSCM along the optical axis (z-axis) is poorer than the lateral counterpart due to the axially elongated shape of the laser focus. The layered features evident

in the xz-images do not therefore represent individual microdomains but arise from sets of several layers.

Somewhat surprisingly, as a result of the induced concentration gradient and thickness profile, we observed that material from the sample center moves toward the edge of the sample. With the capability of LSCM techniques to enable a real-time imaging in a nondestructive manner, we were able to actually observe the movement of microdomains along the radial direction. Figure 3 shows sequential LSCM lateral (xy-plane) images from the same sample used in Figure 2. Three micrographs taken at 20 s intervals at the same sample position show that two adjacent lamellar microdomains (A and B) move along the radial direction (indicated by the arrow), and their boundaries merge together as domain B catches up with domain A. For a 40 s time interval, these domains moved with an average speed of 200 nm/s. Since the sample shown in Figures 2 and 3 is a viscous lyotropic BCP, the shear force exerted by

the surface of glass substrate should be a function of the distance from the sample surfaces as well as a function of the local concentration of the solvent. Utilizing the real-time, real-space imaging capability of LSCM technique, further study will follow on the evolution and the dynamic behavior of BCP morphologies.

In summary, this work demonstrates that LSCM can provide detailed 3-D optical imaging of ultrahigh molecular weight BCPs having lamellar and cylindrical morphologies. Without need for any sophisticated sample preparation steps (e.g., microtome and/ or staining for TEM), structural details of lamellar microdomains of as-cast SI_{LAM} were successfully obtained in 3-D by LSCM. Through depth profiling of the annealed SI_{CYL} specimen, grains of the cylindrical domains are found to be oriented parallel to the surface at the vicinity of glass substrate but more randomly ordered near the center of the specimen. Because of the fast scanning capability and noninvasive nature of the confocal imaging technique, LSCM can also be used to explore the dynamics of BCP phase behavior. In the present study, the motion of microdomains during drying of a lamellar gel sample was visualized by LSCM.

Supporting Information Available: Reflection mode LSCM images (*xy*-scan) of a dried and annealed SI_{CYL} specimen showing the PS cylindrical domains in a 50 μm film between glass substrates. This material is available free of charge via the Internet at http://pubs.acs.org.

References and Notes

(1) Thomas, E. L.; Lescanec, R. L. *Philos. Trans. R. Soc. London A* **1994**, *348*, 149−166.

(2) Park, C.; Yoon, J.; Thomas, E. L. *Polymer* **2003**, *44*, 6725−6760.

(3) Thomas, E. L. *The Encyclopedia of Polymer Science and Engineering*; John Wiley: New York, 1986; Vol. 5.

(4) Urbas, A. M.; Maldovan, M.; DeRege, P.; Thomas, E. L. *Adv. Mater.* **2002**, *14*, 1850−1853.

(5) Hamley, I. W.; Connell, S. D.; Collins, S. *Macromolecules* **2004**, *37*, 5337−5351.

(6) Harrison, C.; Adamson, D. H.; Cheng, Z.; Sebastian, J. M.; Sethuraman, S.; Huse, D. A.; Register, R. A.; Chaikin, P. M. *Science* **2000**, *290*, 1558.

(7) Schwark, D. W.; Vezie, D. L.; Reffner, J. R.; Thomas, E. L.; Annis, B. K. *J. Mater. Sci., Lett.* **1992**, *11*, 352.

(8) Chen, J. T.; Thomas, E. L. *J. Mater. Sci.* **1996**, *31*, 2531−2538.

(9) Fasolka, M. J.; Goldner, L. S.; Hwang, J.; Urbas, A. M.; DeRege, P.; Swager, T.; Thomas, E. L. *Phys. Rev. Lett.* **2003**, 90, 016107/1−016107/4.

(10) Balsara, N. P.; Hammouda, B.; Kesani, P. K.; Jonnalagadda, S. V.; Straty, G. C. *Macromolecules* **1994**, *27*, 2566−2573.

(11) Cohen, Y.; Albalak, R. J.; Dair, B. J.; Capel, M. S.; Thomas, E. L. *Macromolecules* **2000**, *33*, 6502−6516.

(12) Shin, G.; Sakamoto, N.; Saijo, K.; Suehiro, S.; Hashimoto, T.; Amemiya, Y. *Macromolecules* **2000**, *33*, 9002−9014.

(13) Halbhuber, K. J.; Konig, K. *Ann. Anat.* **2003**, *185*, 1−20.

(14) Sokol, D. L.; Zhang, X.; Lu, P.; Gewirtz, A. M. *Proc. Natl. Acad. Sci. U.S.A.* **1998**, *95*, 11538−11543.

(15) Sharpe, J.; Ahlgren, U.; Perry, P.; Hill, B.; Ross, A.; Hecksher-Sorensen, J.; Baldock, R.; Davidson, D. *Science* **2002**, *296*, 541−545.

(16) van Blaaderen, A.; Rue, R.; Wiltzius, P. *Nature (London)* **1997**, *385*, 321−324.

(17) Lee, W.; Chan, A.; Bevan, M. A.; Lewis, J. A.; Braun, P. V. *Langmuir* **2004**, *20*, 5262−5270.

(18) Held, G. A.; Kosbar, L. L.; Dierking, I.; Lowe, A. C.; Grinstein, G.; Lee, V.; Miller, R. D. *Phys. Rev. Lett.* **1997**, *79*, 3443−3446.

(19) Hirokawa, Y.; Jinnai, H.; Nishikawa, Y.; Okamoto, T.; Hashimoto, T. *Macromolecules* **1999**, *32*, 7093−7099.

(20) Jinnai, H.; Koga, T.; Nishikawa, Y.; Hashimoto, T.; Hyde, S. T. *Phys. Rev. Lett.* **1997**, *78*, 2248−2251.

(21) Yoon, J.; Lee, W.; Thomas, E. L. *MRS Bull.* **2005**, *30*, 721−726.

(22) Urbas, A.; Fink, Y.; Thomas, E. L. *Macromolecules* **1999**, *32*, 4748−4750.

(23) Deng, T.; Chen, C.; Honeker, C.; Thomas, E. L. *Polymer* **2003**, *44*, 6549−6553.

(24) Yoon, J.; Lee, W.; Thomas, E. L. *Adv. Mater.* **2006**, *18*, 2691−2694.

(25) Paddock, S. W. *Biotechniques* **2002**, *32*, 274.

(26) Shibayama, M.; Hashimoto, T.; Hasegawa, H.; Kawai, H. *Macromolecules* **1983**, *16*, 1427−1433.

MA0711341